Department of Mathematics and Systems Analysis

Analyticity of point measurements in inverse conductivity and scattering problems

Otto Seiskari

A!

DOCTORAL DISSERTATIONS

Aalto University publication series
DOCTORAL DISSERTATIONS 165/2013

Analyticity of point measurements in inverse conductivity and scattering problems

Otto Seiskari

A doctoral dissertation completed for the degree of Doctor of Science (Technology) to be defended, with the permission of the Aalto University School of Science, at a public examination held at the lecture hall M1 of the school on 22 November 2013 at 12 o'clock.

Aalto University
School of Science
Department of Mathematics and Systems Analysis
Inverse Problems

Supervising professor
Prof. Nuutti Hyvönen

Thesis advisor
Prof. Nuutti Hyvönen

Preliminary examiners
Prof. Rainer Kress, Georg-August-Universität Göttingen, Germany
Prof. Mikko Salo, University of Jyväskylä, Finland

Opponent
Prof. Gunther Uhlmann, University of Washington, USA

Aalto University publication series
DOCTORAL DISSERTATIONS 165/2013

ISBN 978-952-60-5383-7
ISBN 978-952-60-5384-4 (pdf)
ISSN-L 1799-4934
ISSN 1799-4934 (printed)
ISSN 1799-4942 (pdf)
http://urn.fi/URN:ISBN:978-952-60-5384-4

Unigrafia Oy
Helsinki 2013

Finland

Aalto University

Abstract

Aalto University, P.O. Box 11000, FI-00076 Aalto www.aalto.fi

Author
Otto Seiskari

Name of the doctoral dissertation
Analyticity of point measurements in inverse conductivity and scattering problems

Publisher School of Science

Unit Department of Mathematics and Systems Analysis

Series Aalto University publication series DOCTORAL DISSERTATIONS 165/2013

Field of research Mathematics

Manuscript submitted 28 May 2013 **Date of the defence** 22 November 2013

Permission to publish granted (date) 4 September 2013 **Language** English

☐ **Monograph** ☒ **Article dissertation (summary + original articles)**

Abstract

Inverse conductivity and Helmholtz scattering problems with distributional boundary values are studied. In the context of electrical impedance tomography (EIT), the considered concepts can be interpreted in terms of measurements involving point-like electrodes.

The notion of *bisweep data* of EIT, analogous to the *far-field pattern* in scattering theory, is introduced and applied in the theory of inverse conductivity problems. In particular, it is shown that bisweep data are the Schwartz kernel of the relative Neumann-to-Dirichlet map, and this result is employed in proving new partial data results for Calderón's problem. Similar techniques are also applied in the scattering context in order to prove the joint analyticity of the far-field pattern.

Another recent concept, *sweep data* of EIT, analogous to the far-field backscatter data, is studied further, and a numerical method for locating small inhomogeneities from sweep data is presented. It is also demonstrated how bisweep data and conformal maps can be used to reduce certain numerical inverse conductivity problems in piecewise smooth plane domains to equivalent problems in the unit disk.

Keywords Inverse problems, electrical impedance tomography, point measurements, Calderón problem, partial data, (bi)sweep data, elliptic boundary value problems, scattering, far-field pattern

ISBN (printed) 978-952-60-5383-7 **ISBN (pdf)** 978-952-60-5384-4

ISSN-L 1799-4934 **ISSN (printed)** 1799-4934 **ISSN (pdf)** 1799-4942

Location of publisher Helsinki **Location of printing** Helsinki **Year** 2013

Pages 118 **urn** http://urn.fi/URN:ISBN:978-952-60-5384-4

Aalto-yliopisto

Tiivistelmä

Aalto-yliopisto, PL 11000, 00076 Aalto www.aalto.fi

Tekijä
Otto Seiskari

Väitöskirjan nimi
Pistemittausten analyyttisyys käänteisjohtavuus ja -sirontaongelmissa

Julkaisija Perustieteiden korkeakoulu

Yksikkö Matematiikan ja systeemianalyysin laitos

Sarja Aalto University publication series DOCTORAL DISSERTATIONS 165/2013

Tutkimusala Matematiikka

Käsikirjoituksen pvm 28.05.2013 **Väitöspäivä** 22.11.2013

Julkaisuluvan myöntämispäivä 04.09.2013 **Kieli** Englanti

☐ **Monografia** ☒ **Yhdistelmäväitöskirja (yhteenveto-osa + erillisartikkelit)**

Tiivistelmä

Väitöskirjassa tutkitaan käänteisjohtavuusongelmia ja Helmholtzin yhtälön sirontaongelmia distributionaalisilla reuna-arvoilla. Impedanssitomografian (EIT) tapauksessa nämä voidaan tulkita mittauksina pistemäisillä elektrodeilla.

Työssä esitellään uusi, käänteissirontateorian *kaukokentän* kaltainen käsite, EIT:n *bisweep-data*, jota voidaan hyödyntää käänteisjohtavuusongelmien teoriassa. Erityisesti näytetään, että bisweep-data on suhteellisen Neumann-to-Dirichlet-kuvauksen Schwartzin ydin, minkä avulla todistetaan uusia osittaisdatatuloksia Calderónin ongelmalle. Vastaavia tekniikoita sovelletaan myös sirontateoriassa ja osoitetaan kaukokenttäkuvauksen yhdistetty analyyttisyys.

Lisäksi väitöskirjassa tutkitaan toista hiljattain esiteltyä käsitettä, kaukokentän takaisinsirontadatan tyyppistä EIT:n *sweep-dataa* ja laaditaan numeerinen menetelmä pienten epähomogeenisuuksien paikantamiseen sweep-datan avulla. Työssä näytetään myös, kuinka bisweep-datan ja konformikuvausten avulla tietyt numeeriset käänteisjohtavuusongelmat voidaan palauttaa paloittain sileistä tason alueista yksikkökiekkoon.

Avainsanat Inversio-ongelmat, impedanssitomografia, pistemittaukset, Calderónin ongelma, osittainen data, (bi)sweep-data, elliptiset reuna-arvo-ongelmat, sironta, kaukokenttä

ISBN (painettu) 978-952-60-5383-7 **ISBN (pdf)** 978-952-60-5384-4

ISSN-L 1799-4934 **ISSN (painettu)** 1799-4934 **ISSN (pdf)** 1799-4942

Julkaisupaikka Helsinki **Painopaikka** Helsinki **Vuosi** 2013

Sivumäärä 118 **urn** http://urn.fi/URN:ISBN:978-952-60-5384-4

Preface

First and foremost, I would like to express my gratitude to my thesis instructor and supervisor Nuutti Hyvönen for constant support, great advice, and exceptional dedication throughout the process. In addition, I would like to thank all members of the inverse problems group for help, inspiring discussions, and a relaxed working environment. Thanks are also due to Olavi Nevanlinna and Marko Huhtanen from whom I learned a lot during the earlier stages of my studies.

For the financial support of this thesis, I am indebted to the Academy of Finland (decision 140998), TEKES — the Finnish Funding Agency for Technology and Innovation (contract 40370/08), as well as FICS — the Finnish Doctoral Programme in Computational Sciences. I am also grateful to Rainer Kress and Mikko Salo, the preliminary examiners of the thesis, for their time and valuable comments. Finally, I would like to thank my friends and family, especially my parents Johanna and Pekka, for joyful moments and continuous support.

Espoo, September 5, 2013,

Otto Seiskari

Contents

List of publications

This thesis consists of an overview and of the following publications which are referred to in the text by their Roman numerals.

[I] Hyvönen, N., and Seiskari, O. Detection of multiple inclusions from sweep data of electrical impedance tomography. *Inverse Problems*, Vol. 28, 095014 (22 pp.), 2012.

[II] Hyvönen, N., Piiroinen, P., and Seiskari, O. Point measurements for a Neumann-to-Dirichlet map and the Calderón Problem in the plane. *SIAM Journal on Mathematical Analysis*, Vol. 44, No. 5, pp. 3526–3536, 2012.

[III] Griesmaier, R., Hyvönen, N., and Seiskari, O. A note on analyticity properties of far field patterns. *Inverse Problems and Imaging*, Vol. 7, No. 2, pp. 491–498, 2013.

[IV] Seiskari, O. Point electrode problems in piecewise smooth plane domains. *arXiv:1212.5424*, 24 pp., May 2013.

Author's contribution

Publication I: "Detection of multiple inclusions from sweep data of electrical impedance tomography"

This article is based on my Master's thesis [49]. I conducted the majority of the numerical experiments, and the new theoretical results were devised by me, but with considerable help and guidance from Hyvönen.

Publication II: "Point measurements for a Neumann-to-Dirichlet map and the Calderón Problem in the plane"

I participated in the whole writing process. More specifically, I formulated the proof of joint analyticity with respect to two complex variables (§3.1), the factorization (§3.2), and also contributed to the material in Section 3.4.

Publication III: "A note on analyticity properties of far field patterns"

I also participated in the majority of the writing process of this article. I devised the original versions of Lemma 3.3 and the proof of Theorem 2.2 using trigonometric charts for the sphere surfaces. In the final version of the paper, these have been reformulated for projective charts by Griesmaier.

Publication IV: "Point electrode problems in piecewise smooth plane domains"

This is my own work

1. Introduction

Inverse problems

In the 1920's, Jacques Hadamard stated three conditions for a *well-posed* mathematical problem: A solution must exist, be unique, and depend continuously on the input data in some reasonable topology. The approximate meaning of the last condition is that small errors in the data should cause only small errors in the solution. Problems that fail to satisfy all these conditions are called *ill-posed* in the sense of Hadamard — who disbelieved that they could represent any meaningful, resolvable questions of physical nature.

However, it appears that many interesting questions in mathematical physics are ill-posed. A notable group are *inverse problems*, which are "backwards" versions of certain mathematical questions, usually related to partial differential equations. A classical example is the backward heat equation, where the *forward problem* is: given the heat distribution in an object now, how does it look like in one second? The forward problem is well-posed. However, the inverse problem: given the heat distribution now, determine how it was one second ago; is highly ill-posed: miniscule perturbations in the current state could correspond to arbitrarily large changes in the solution. This type of noise-amplifying phenomena appear to prevent solving ill-posed inverse problems with any inaccuracies in the input, and some level of noise is present in essentially all real-life data.

Fortunately, many ill-posed problems can be solved in a stable manner applying *regularization*, an approach pioneered by A. N. Tikhonov in the 1960's. Even if a problem is ill-posed, it can nevertheless be possible to construct a *regularization strategy* that allows for stable reconstructions which can be shown to converge to a correct solution as the noise level diminishes to zero. In some sense, this serves as a counterexample showing that Hadamard's criteria

were too strict. From a practical perspective, regularization can be seen as a compromise between stability and resolution.

Another framework for solving ill-posed problems is *statistical inversion*, where prior probabilistic information about the solution is combined with the measurements using Bayes' formula. This is a flexible approach, in which well-posedness of the problem is not required. However, Bayesian computations can be challenging. For instance, the mathematical formulation of a *maximum a posteriori* solution estimator is straightforward, yet finding it algorithmically can be slow and difficult. In some cases, statistical estimators can also be shown equivalent to certain regularization schemes.

Electrical impedance tomography

Electrical impedance tomography (EIT) aims to recover the position-dependent electrical properties of an object from measurements on its boundary. In practice, one attaches multiple electrodes on the surface of a body and drives different patterns of electric current through them, measuring the resulting voltages on the electrodes. A reconstruction algorithm is then applied to the measured data to produce an approximate map of the *conductivity*, and occasionally also the *permittivity*, of the object.

EIT has a variety of current and prospective applications in, among others, medicine, non-destructive material testing, industrial process monitoring, and geological imaging [2][7][52]. It has several potential advantages over other imaging modalities. For example, the conductivity of certain tumors differs from healthy tissue by orders of magnitude, whereas their contrasts in X-ray or ultrasound images are negligible. Other potential benefits of EIT in medicine, in comparison to techniques such as computer tomography (CT) and magnetic resonance imaging (MRI), include inexpensive equipment and safety.

In geophysics, EIT is commonly known as electrical resistivity tomography (ERT), and electrical capacitance tomography (ECT) is a slightly different but related modality, with applications in industrial process monitoring. Mathematically, impedance tomography involves *inverse conductivity problems* that are highly non-linear and ill-posed by nature. As a result, EIT is inherently a low-resolution method and an unlikely candidate for a successful general-purpose tomographic technique, such as X-ray imaging.

One mathematical aspect of the theory of EIT is to consider under which assumptions idealized (continuum) measurements can determine the conductivity of an object. Another challenge is to develop methods for reconstructing it from

actual noisy and finite measurements. The study of the idealized models involves challenging problems which are of interest as fundamental mathematical research. Furthermore, this mathematical theory is closely related to neighboring inverse problem topics, such as inverse scattering and optical tomography. Thus the mathematical machinery in these fields can advance EIT theory and vice versa. Section 3 presents the essentials of EIT from the perspective of this thesis.

Inverse scattering

Indirectly observing objects and structures from scattered waves is a common and important approach in physics and many applications. Scattering techniques are used to study phenomena of both small and large scales. Examining microscopic crystalline structures using X-rays and locating oil reserves by measuring seismic waves are both based on this idea. An umbrella term for the resulting mathematical problems is *inverse scattering*.

The basic concepts of scattering theory for the Helmholtz equation are presented in Section 4. The introduction is brief due to the rather narrow view considered in this thesis. Comprehensive reviews of the subject can be found in [10][11][33] and the references therein.

Analyticity

Analyticity is a strong elementary mathematical property that links the local behavior of a function to its global values. An analytic function on the real line is determined by its values on any non-empty open interval. This concept is also intimately connected to the notions of harmonicity (Laplace's equation) and complex differentiability.

In multiple dimensions, the concept of *joint* and *separate* analyticity (and smoothness) have been a source of confusion since the days of Cauchy, who erred to claim [34] that all separately continuous functions are continuous (they are not, see counterexample on page 13). These concepts are introduced in Section 2.

Outline

Most of this thesis studies the theoretical aspects of inverse conductivity problems with *point electrodes* (cf. Section 3.6). In this approach, current-feeding electrodes are modeled as point sources and measuring electrodes are defined to evaluate the voltage perturbation caused by an inclusion, that is, an area in which the conductivity deviates from homogeneous background. The notion of *bisweep data* of EIT, an analogous concept to the *far-field pattern* in inverse scattering, is introduced.

The main results in this thesis are based on the idea of considering the analytic properties of measurements with respect to the motion of the point electrodes. This allows for a new approach to partial data results for inverse conductivity problems. Similar mathematical methods are also applied to inverse scattering in [**III**]. For some of the published results, more elementary proofs exist, which is discussed in Section 5.

Numerical methods based on bisweep data and *sweep data*, a notion analogous to the backscatter data in inverse scattering, are also considered. The methods rely on the availability of accurate difference data (cf. Section 3.4) and should be regarded as possible new approaches rather than readily applicable algorithms for practical EIT reconstructions.

2. Some notes on analyticity

2.1 Joint and separate real analyticity

Let $D \subset \mathbb{R}^n$ be a non-empty open set. A function $f : D \to \mathbb{R}$ is said to be (jointly) *analytic* if, for all $x_0 \in D$, the multidimensional Taylor series

$$\sum_{\alpha} \frac{(D^\alpha f)(x_0)}{\alpha!}(x - x_0)^\alpha$$

converges to $f(x)$ for all x in some neighborhood of x_0. This is sometimes denoted $f \in \mathscr{C}^\omega(D)$ or $f \in \mathcal{A}(D)$. All such functions are of class $\mathscr{C}^\infty$ (smooth) but the converse is not true. Analytic functions can also be defined on *analytic manifolds*, that is, manifolds whose transition maps are analytic functions. [43][44]

A function $f : \mathbb{R}^n \to \mathbb{R}$ is *separately* analytic if $f(x_1, \ldots, x_n)$ is analytic with respect to each variable x_j, $j = 1, \ldots, n$ when the other variables assume arbitrary, fixed values. Separate analyticity in an Euclidean space $\mathbb{R}^n$ does *not* imply joint analyticity, as shown by the well-known counterexample [34]

$$f(x,y) = \begin{cases} 0 & \text{if } (x,y) = (0,0) \\ \frac{xy}{x^2+y^2} & \text{otherwise,} \end{cases} \tag{2.1}$$

which is discontinuous at the origin. Even smooth separately analytic functions are not necessarily jointly analytic. A counterexample is given by [34]

$$f(x,y) = \begin{cases} 0 & \text{if } (x,y) = (0,0) \\ xy\, e^{-\frac{1}{x^2+y^2}} & \text{otherwise.} \end{cases}$$

Joint analyticity is thus truly a stronger condition than separate analyticity. The nature of the singularities of separately analytic functions has been studied in, for example, [3] and [34].

2.2 Holomorphy

Let $D \subset \mathbb{C}$ be open and non-empty. A function $f : D \to \mathbb{C}$ is called *complex analytic* or *holomorphic* if the complex derivative

$$\frac{\mathrm{d}f}{\mathrm{d}z}(z) := \lim_{h \to 0} \frac{f(z+h) - f(z)}{h} \tag{2.2}$$

exists at every $z \in D$. The existence of a complex derivative implies the existence and analyticity of complex derivatives of any order. Similarly to the real case, one can define the notions of joint and separate analyticity of complex functions $f : \mathbb{C}^n \to \mathbb{C}$ in multiple variables. However, an important result, Hartog's Theorem, reveals that these are, in fact, equivalent; a separately analytic complex function is always jointly analytic. [27][44]

Hartog's Theorem can be a useful tool when studying joint analyticity of real functions in several variables. Namely, if one can show that $f : \mathbb{R}^n \to \mathbb{R}$ is the restriction of a complex analytic function $g : \mathbb{C}^n \to \mathbb{C}$ to $\mathbb{R}^n \cong \{(z_1, \ldots, z_n) \in \mathbb{C}^n : \Im z_1 = \ldots = \Im z_n = 0\}$, it follows that f is jointly analytic. This is especially convenient if the separate analyticity of g is revealed by (2.2), which is the case in all the publications included in this thesis. Unlike some mathematical techniques, such as conformal mapping of electrostatic problems, this method is not inherently restricted to the study of physical configurations that can be reduced to two space dimensions, as also demonstrated in [**III**].

2.3 Analytic continuation

A central property is that an analytic function in $\mathbb{R}^n$ (the same is true in $\mathbb{C}^n$, on analytic manifolds, and various connected subsets of these) is defined by its values on an arbitrary non-empty open set, or equivalently, the partial derivatives of all multi-orders at any point. [43]

However, joint analyticity is not a necessary condition for possessing this property. For example, the knowledge of the values of a separately analytic function $f : \mathbb{R}^n \to \mathbb{R}$ on an arbitrary open subset Ω of $\mathbb{R}^n$ reveals the whole function. It is recovered by first analytically extending f along the first axis into the set

$$\{(x_1, x_2, \ldots, x_n) \in \mathbb{R}^n \,:\, (x, x_2, \ldots, x_n) \in \Omega \text{ for some } x \in \mathbb{R}\}$$

and so forth.

3. Electrical impedance tomography

This section describes the forward models that are considered in this thesis, together with some remarks and examples regarding inverse conductivity problems and different electrode models. EIT is also studied in setups that do not strictly fit into the following definitions, for instance, in unbounded domains.

3.1 Continuum forward model

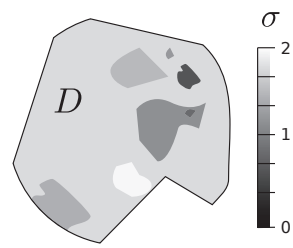

Let $D \subset \mathbb{R}^n$, $n \geq 2$ be a bounded Lipschitz domain with a connected complement. In EIT, electricity inside the domain is modeled by the *conductivity equation*,

$$\nabla \cdot (\sigma \nabla u) = 0 \quad \text{in } D, \tag{3.1}$$

where the *conductivity* $\sigma \in L^\infty(D)$ is assumed to be bounded away from zero, $\sigma \geq c > 0$ in D, and u is the potential of the electric field. Essentially, (3.1) states that there are no sources of electric current inside the body D. The equation is a highly accurate approximation for static (direct input currents) or low-frequency time-harmonic potentials u. In the latter case, which corresponds to sinusoidal alternating input currents, σ is replaced with a frequency-dependent complex *admittivity*, usually denoted γ, and the values of u are complex *phasors*. It is also possible to study anisotropic materials by letting the values of σ be positive-definite matrices. [2][52] In what follows, a real and isotropic conductivity is assumed, unless otherwise stated.

With a Neumann boundary condition $\sigma \frac{\partial u}{\partial \nu} = f$ on ∂D, Equation 3.1 has a solution if and only if $\int_{\partial D} f \, \mathrm{d}s = 0$. Physically, f represents the signed density of outgoing current on the boundary, and the integral must be zero due to conservation of current. We use a diamond subscript to denote subspaces of functions with vanishing mean, and interpret integrals over ∂D as dual

evaluations with a constant function, if necessary. For example,

$$H_\diamond^{-1/2}(\partial D) := \{f \in H^{-1/2}(\partial D) \,:\, \langle f, 1\rangle_{H^{-1/2}(\partial D)\times H^{1/2}(\partial D)} = 0\}.$$

Furthermore, the subscript in the angle brackets denoting dual evaluation is routinely omitted or simplified as, for instance, $\langle\cdot,\cdot\rangle_{\partial D}$ when the spaces are irrelevant (in the sense of Gelfand triples) or clear from the context. For the definitions and basic properties of the Sobolev spaces H^s, refer to, e.g., [48].

The solution to the Neumann problem of (3.1) is unique up to an addition of a constant function, which represents the arbitrary potential ground level in the physical context. For example, if $f \in H_\diamond^{-1/2}(\partial D)$, then there exists a unique function equivalence class

$$u \in H^1(D)/\mathbb{R} := \{\{v + C \,:\, C \in \mathbb{R}\} \,:\, v \in H^1(D)\}$$

that satisfies the weak Neumann problem

$$\int_D \sigma\nabla u \cdot \nabla v \,\mathrm{d}x = \langle f, \gamma v\rangle_{\partial D} \qquad \text{for all } v \in H^1(D)/\mathbb{R},$$

where the trace operator $\gamma : H^1(D)/\mathbb{R} \to H^{1/2}(\partial D)/\mathbb{R} = (H_\diamond^{-1/2}(\partial D))'$ is the unique bounded functional that coincides with taking the Dirichlet boundary value for continuous functions.

Thus one can define the *Neumann-to-Dirichlet map* (current-to-voltage map)

$$\Lambda_\sigma : H_\diamond^{-1/2}(\partial D) \to H^{1/2}(\partial D)/\mathbb{R}, \quad f \mapsto \gamma u.$$

In the continuum forward model, one assumes that Λ_σ, or equivalently its inverse, the Dirichlet-to-Neumann map Λ_σ^{-1}, is known from the measurements. It should be noted that many theoretical papers use the opposite convention of denoting the Dirichlet-to-Neumann map by Λ_σ.

3.2 Calderón problem

The inverse problem for the continuum forward model, called *Calderón's inverse conductivity problem*, is as follows: Given the measurement operator Λ_σ, is it possible to determine the conductivity $\sigma \in L^\infty(D)$? Research on this question was pioneered by Calderón, who proposed it in [6], together with a linearization-based algorithm for reconstruction.

The first global uniqueness result for dimensions $n \geq 3$ was given by Sylvester and Uhlmann [51] for smooth conductivities and domains $D \subset \mathbb{R}^n$ (see also [40][41] for earlier uniqueness results for analytic and piecewise analytic conductivities). In the plane, $n = 2$, it was shown by Nachman [47] that $\sigma \in W^{2,p}(D)$,

$p > 1$ is uniquely determined by Λ_σ in Lipschitz domains. The regularity assumptions for σ and D have since been reduced significantly; see [52] and the references therein. In particular, Astala and Päivärinta [1] proved that any $\sigma \in L^\infty(D)$ with a positive lower bound is determined by Λ_σ in any simply-connected domain $D \subset \mathbb{R}^2$, thus giving an affirmative answer to the inverse conductivity problem in the plane.

In the original formulation [6], Calderón also enquired the existence of an algorithm for finding σ (based on the knowledge of Λ_σ^{-1}). Even though many of the uniqueness proofs are constructive, they may not directly yield numerical schemes for reconstructing conductivities, let alone methods suitable for noisy and discrete data. There are results that guarantee stable reconstruction under some *a priori* constraints on σ in the sense of a regularization strategy. In the plane, the $\bar{\partial}$-method (D-bar method) can be used to construct a family $\{\Gamma_\alpha\}_{\alpha>0}$ of functions such that $\|\Lambda^{-1} - \Lambda_\sigma^{-1}\|_{H^{1/2}(\partial D)\to H^{-1/2}(\partial D)} < \epsilon$ implies [39]

$$\|\Gamma_{\alpha(\epsilon)}\Lambda^{-1} - \sigma\|_{\mathscr{C}(\overline{D})} < \alpha(\epsilon) \xrightarrow{\epsilon\to 0} 0$$

for any fixed σ of class $\mathscr{C}^2$ that is homogeneous near the boundary (cf. equation 3.2 on page 24).

Numerous other algorithms can also provably deduce limited information on σ. A notable example is the factorization method [15][18], which can, under certain restrictions, find the support of an inclusion $\operatorname{supp}(1-\sigma) \subset\subset D$ and also has a proven regularization strategy [45]. It was originally adapted to EIT by Brühl and Hanke [4][5] from a similar method developed for inverse scattering by Kirsch [38]. The factorization method is applied and discussed in more detail in [**IV**].

There are also recent studies concerning Calderón problem with partial data, e.g., [29][30][36][37]. That is, under which conditions it is possible to recover σ from data with restrictions on the supports of the current patterns f (respectively voltage patterns) and the portion of the boundary ∂D where the corresponding voltages (resp. currents) are measured. This subject is considered in [**II**] and [**IV**].

3.3 Electrode models

In a typical EIT measurement setup, a relatively small number of electrodes, modeled as $E_1, \ldots, E_N \subset \partial D$, are placed on the boundary of an object D (see Figure 3.1a). The potentials $U^k = (U_1^k, \ldots, U_N^k) \in \mathbb{R}^N/\mathbb{R}$ on the electrodes are then measured with as many linearly independent current patterns $I^k =$

$(I_1^k, \dots, I_N^k) \in \mathbb{R}^N_\diamond$ as possible ($k = 1, \dots, N-1$ to be exact).

The central question is how these discrete measurements relate to the continuum model and the Neumann-to-Dirichlet map Λ_σ. A naive approach is to view the current pattern I as a discretization of a continuous function $f = \sigma \frac{\partial u}{\partial \nu}$, which could be approximated by interpolating certain current densities derived[1] from I. The resulting electrode potentials U are then modeled by the point values of $u|_{\partial D} = \Lambda_\sigma f$ at the electrodes. This discretization is sometimes called the continuum model.[2] Unfortunately, it is highly inaccurate [7][9]. A straightforward improvement is to note that current cannot travel through ∂D outside the electrodes. Combined with the assumption of constant current density on each electrode, this yields the *gap model* (a.k.a. ave-gap model), which can also be viewed as a discretization of Λ_σ using a certain basis of current and voltage patterns.

However, there are two more phenomena that significantly affect the measurement. Especially if large portions of the boundary ∂D are covered by electrodes, which are made of highly conductive materials, then the electrodes themselves form a low-resistance path for the current. As a result, the current density through an electrode interface will not be constant. This is taken into account by the *shunt model*, in which the potential is assumed to be constant $u|_{E_j} = U_j$ on each E_j, while the current density vanishes outside the electrodes. This results in a mixed Neumann–Dirichlet forward model that does not readily correspond to a discretization of Λ_σ.

The boundary current densities are limited by a phenomenon called *contact impedance* (contact resistance), which is caused by a thin, highly resistive layer on the contact interfaces of the electrodes and the object. All the aforementioned effects are taken into account by the *complete electrode model* (CEM) [9][50]:

$$\begin{cases} \nabla \cdot (\sigma \nabla u) = 0 & \text{in } D, \\ u + z\sigma \frac{\partial u}{\partial \nu} = U_j & \text{on } E_j,\ j = 1, \dots, N, \\ \frac{\partial u}{\partial \nu} = 0 & \text{on } \partial D \setminus \bigcup_{j=1}^N E_j, \\ \int_{E_j} \sigma \frac{\partial u}{\partial \nu} \, \mathrm{d}s = I_j, & j = 1, \dots, N, \end{cases}$$

[1] In the following numerical examples involving the "continuum" model, the value $f(e_j)$ of the interpolant at the midpoint e_j of an electrode is set to $I_j/|E_j|$ (as in [9]). This choice of scaling is not the only possibility and hardly the best one, as suggested by Figure 3.2b.

[2] It is also common to consider discretizations of the Dirichlet-to-Neumann map Λ_σ^{-1} as a forward model and approximate the boundary potential $u|_{\partial D}$ by a continuous function whose values at the electrodes are given by U. The resulting modeling error is comparable to that of the Neumann-to-Dirichlet "continuum" and gap models.

where $z : \partial D \to (c, \infty)$, $c > 0$, models the contact impedance. For any $I \in \mathbb{R}^N_\diamond$, the above equations have a unique solution $(u, U) \in (H^1(D) \times \mathbb{R}^N)/\mathbb{R}$ [50], and the measurement operator $R_\sigma : \mathbb{R}^N_\diamond \to \mathbb{R}^N/\mathbb{R}$, $I \mapsto U$ can be identified with a symmetric $(N-1) \times (N-1)$ matrix, which depends on σ, $E_1, \ldots, E_N$, and z. At best, the CEM can correctly match EIT measurements up to instrument precision [7][50]. Alternatively, contact impedances may be modeled by augmenting the gap or shunt models with "lumped" contact resistances Z_j (whence $U_j \approx u|_{E_j} + Z_j I_j$), but the resulting models are not as accurate as the CEM [7].

Figure 3.1 illustrates the EIT forward problem with an example and compares several different electrode models. The figures are based on numerical data simulated using finite element and boundary layer methods. The values of the electrode contact impedances used in the computations are comparable to those measured in [9] after appropriate rescaling[3]. Notice the high peaks in the CEM current density near electrode edges, caused by the shunting effect, in Figure 3.1c; for the shunt model, the singularities would be even more severe (cf. [12]).

When the measured potentials U are predicted by the gap model as the values of u at the midpoints $e_1, \ldots, e_N$ of the electrodes (with normalization $\sum_i U_i = 0$), the modeling error $\|U - U^{\mathrm{CEM}}\|_\infty$ reaches 7% of $\|U^{\mathrm{CEM}}\|_\infty$ and the "continuum" model performs even worse. This is quite concerning considering the fact that, in this case (for this current pattern), removing the inclusions altogether would cause a perturbation of approximately 4%. The contrast can certainly be better in other setups, especially if the inclusions are located closer to the electrodes. On the other hand, the presented conductivity phantom is realistic from the perspective of what most EIT inversion methods can and should be able to reconstruct relatively well.

[3] Cheng et al. [9] experimented with a cylindrical saline water tank of radius $R = 15$ cm and observed $\sigma z \approx 2.4$ mm (for different constant-conductivity contents of the tank). Simple scaling analysis shows that these setups can be reduced to unit disk ($R = 1$) configurations where $\sigma = 1$ and $z = 2.4$ mm / 15 cm $= 0.016$.

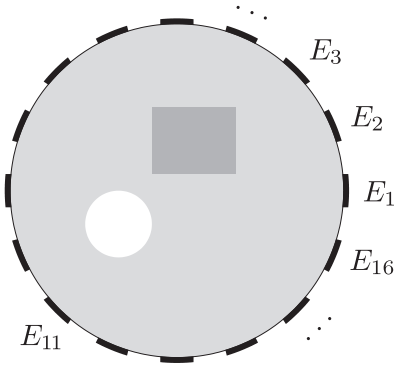

(a) A conductivity phantom σ and 16 electrodes in the unit disk B.

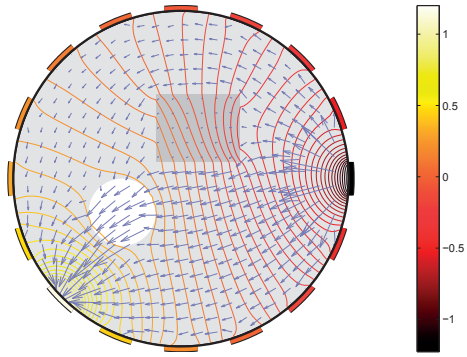

(b) Current density $j = \sigma\nabla u$ (arrows), interior potential u (equipotential lines), and electrode potentials U in the CEM.

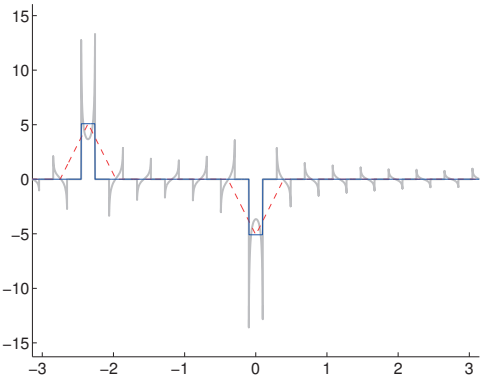

(c) Boundary current densities $f = \sigma\frac{\partial u}{\partial \nu}$ in the CEM (thick gray), gap (blue), and "continuum" (dashed red) models at $(\cos\theta, \sin\theta)$ as functions of θ.

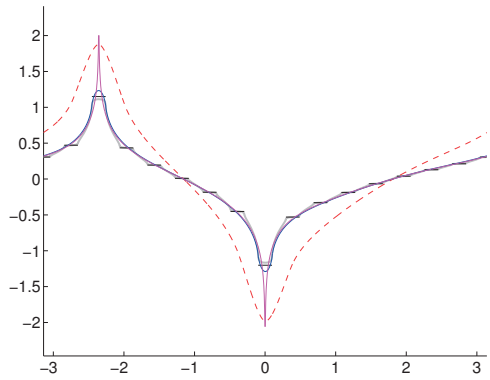

(d) Boundary potentials $u|_{\partial B} = \Lambda_\sigma f$ in different models. The magenta line is $\Lambda_\sigma(\delta_{e_{11}} - \delta_{e_1})$ (cf. §3.6), electrode potentials U of the CEM are shown in black, and the other colors are as in (c).

Figure 3.1. EIT forward problem example. One unit of current is flowing from electrode E_1 to E_{11}. The background conductivity is $\sigma = 1$ and there are two inclusions: a box with $\sigma = 1/10$ and a disk with $\sigma = 10$ (see (a)). Electrode contact impedances have been set to $z = 1/100$. The forward problem (for this current pattern, $I_j = \delta_{j,11} - \delta_{j,1}$, $j = 1, \ldots, 16$) is to determine the electrode potentials $U = (U_1, \ldots, U_{16})$ up to an arbitrary ground level.

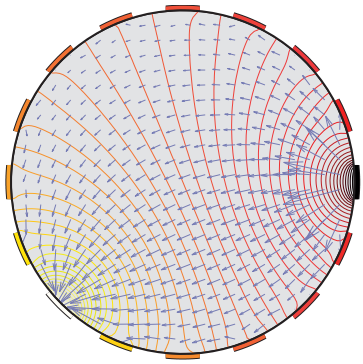

(a) Solution to the homogeneous reference problem corresponding to Figure 3.1b.

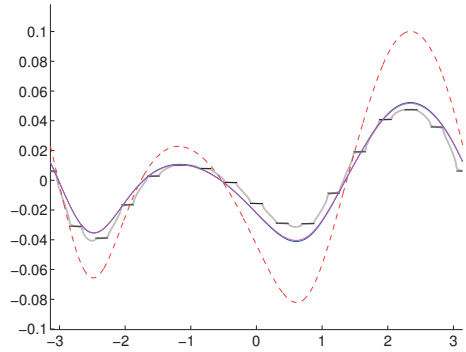

(b) Relative boundary potentials $w|_{\partial B} := (u - u_1)|_{\partial B} = (\Lambda_\sigma - \Lambda_1)f$ and $U - U_1$ in the CEM (colors as in Fig. 3.1d).

Figure 3.2. Difference data example.

3.4 Difference data

Assume that two conductivities σ and $\tilde{\sigma}$ coincide near the boundary:

$$\operatorname{supp}(\sigma - \tilde{\sigma}) \subset\subset D.$$

This framework is relevant if one tries to locate *inclusions*[4] in a known background $\tilde{\sigma}$, for example, homogeneous medium $\tilde{\sigma}(x) = \mathbb{1}(x) := 1$. Possible application could be screening desirably homogeneous media for defects, such as cracks or air bubbles in concrete.

Let Λ_σ, $\Lambda_{\tilde{\sigma}}$ be the Neumann-to-Dirichlet maps of the conductivities. Correspondingly, let R_σ, $R_{\tilde{\sigma}}$ be the respective (CEM) electrode measurement operators, assuming identical contact impedances and electrode configurations. It appears that, even though discretizations of Λ_σ are ill-suited models for R_σ (and real EIT measurements), certain discretizations of the *relative* Neumann-to-Dirichlet map $\Lambda_\sigma - \Lambda_{\tilde{\sigma}}$ are reasonably accurate approximations of the relative operator $R_\sigma - R_{\tilde{\sigma}}$, because various modeling errors tend to "cancel out" in the difference (cf. [42]). Figure 3.2 illustrates this phenomenon. The relative potentials $w|_{\partial B} = (\Lambda_\sigma - \Lambda_{\mathbb{1}})f$ with respect to the setups in Figures 3.1b and 3.2a are shown in Figure 3.2b. If the point values of w at the electrode midpoints in the gap or point electrode ($f = \delta_{e_{11}} - \delta_{e_1}$, cf. Section 3.6) models are used to predict $U - U_{\mathbb{1}}$, the error $\|(U - U_{\mathbb{1}}) - (U^{\mathrm{CEM}} - U_{\mathbb{1}}^{\mathrm{CEM}})\|_\infty$ is below 20% of the perturbation $\|U^{\mathrm{CEM}} - U_{\mathbb{1}}^{\mathrm{CEM}}\|_\infty$. In particular, these discrepancies are an order of magnitude smaller than the error of the gap model in the absolute (non-difference) measurements (cf. Section 3.3).

[4] The perturbation $\sigma - \tilde{\sigma}$ or its support is called an inclusion.

Theoretically, it has been shown in [28], under some simplifying assumptions on σ and D, that as the number N of electrodes is increased and their size decreased in a controlled manner, an approximation of $\Lambda_\sigma - \Lambda_{\tilde{\sigma}} : L^2_\diamond(\partial D) \to L^2(\partial D)/\mathbb{R}$ can be constructed from $R^N_\sigma - R^N_{\tilde{\sigma}}$ so that the discrepancy between these in the operator topology is $\mathcal{O}(d)$, where d is proportional to the maximum distance between adjacent electrode midpoints.

3.5 EIT inverse problems and reconstruction methods

Instead of the infinite Calderón problem discussed in Section 3.2, a practitioner of EIT is faced with the following discrete problem: Given noisy measurements with $\frac{N(N-1)}{2}$ degrees of freedom from N electrodes, determine as much information on σ as possible.

The theoretical aspects of this (CEM-based) inverse problem remain almost unstudied compared to those based on the continuum model. The only fact that seems clear is that no general conductivity σ of any infinite class, such as $\mathscr{C}^k$ or $W^{k,p}$, is uniquely determined by the data[5]. Of course, there are numerous methods for tackling the above problem, many of which yield good qualitative reconstructions. Two examples are presented in Figure 3.3. Current EIT inversion algorithms can be divided into three main classes (cf., e.g., [2][7][46]): *iterative*, *linearized*, and *direct* methods.

Iterative algorithms are based on statistical inversion or related least-squares formulations of discretized versions of the non-linear inverse conductivity problem, which they attempt to solve using Newton-type methods. These are well-suited for the complete electrode model and some can also handle and resolve uncertainties in several quantities such as σ, z or ∂D simultaneously. [13][14][25][46][53] Even though these methods often yield good results, there is no guarantee of global convergence to a meaningful solution. In addition, they can be computationally expensive and slow.

Examples of linearized algorithms include the approach proposed by Calderón [6][31] and one-step methods, such as NOSER [8], which are based on the same formulation as the iterative methods but always stop after the first iteration. One-step methods are widely used in applications and can also employ the complete electrode model [42].

[5]However, if the size and number of electrodes or their positions is allowed to vary (as in, e.g, [16] and [**I**]), the situation changes.

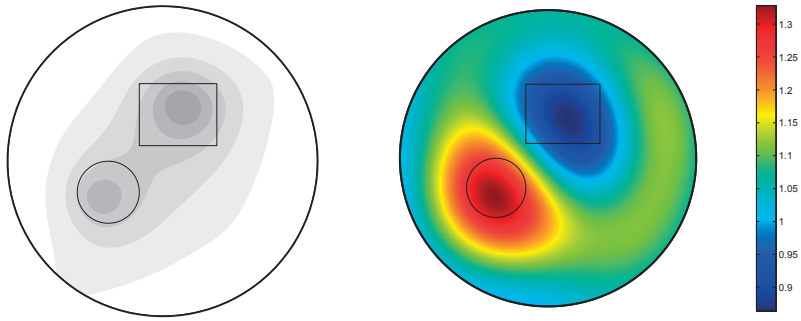

(a) Approximating contours for the inclusions, given by the factorization method (cf. [**IV**]) with 15 eigenvalues and 15 dipole directions.

(b) Reconstruction of σ by Calderón's linearization method [31] with a circular low-pass filter $\chi_{B(0,7)}(\xi)$.

Figure 3.3. Two reconstruction from difference data corresponding to Figures 3.1 and 3.2 with 0.1% measurement noise[6]. The black lines show the actual inclusion boundaries.

The third class comprises of methods that are not based on linearization or (Newton-type) iteration. It contains, among others, the factorization and D-bar methods [15][39][45], which attack some version of the non-linear problem and have a strong theoretical backing. A major drawback of these algorithms is that they generally assume the availability of (some discrete approximation of) $\Lambda_\sigma - \Lambda_{\mathbb{1}}$ (or $\Lambda_\sigma^{-1} - \Lambda_{\mathbb{1}}^{-1}$) as the measurement operator. Because of reasons discussed in Section 3.4, the direct methods are thus often difficult to apply in practice unless the conductivity is homogeneous and known near the boundary, and, in addition to the measurements corresponding to an unknown σ (i.e., the measurement operator R_σ, cf. Section 3.3), one has access to an accurate approximation of the reference measurement operator $R_{\mathbb{1}}$.

In principle, the reference operator can be simulated using the CEM if the shape D, the contact impedances z, and the configuration of the electrodes are known. However, small geometrical modeling errors or incorrect contact impedance values can be much more significant in R_σ than the perturbation caused by the conductivity [42], but in some cases, it may be possible to recover a useful approximation of the background operator from the data (cf., e.g., [32]).

There are also different approaches to eliminating the requirement of a refer-

[6] Uncorrelated additive Gaussian noise with standard deviation $0.001 \cdot \max_k \|U^k\|_\infty$ (with normalization $\sum_j U_j^k = 0$) was added to all components of U^k and U_1^k, $k = 1, \ldots, N-1$. This "0.1%" measurement error corresponds to a relative noise level of approximately 8% in the difference data $U^k - U_1^k$ of this setup.

ence measurement with a homogeneous object. Impractical reference data are not required at all by *time-difference* and *frequency-difference* setups, in other words, relative measurements of conductivities that vary in time or with AC frequency. These have been applied in EIT (cf., e.g., [7]) with linearized methods (also linearized and iterative methods can be used with and benefit from the availability of difference data), but the corresponding non-linear problems lack an established theoretical basis, although some results do exist (see, e.g., [24]). In general, this remains a future challenge for direct EIT methods.

3.6 Point electrode measurements

As discussed in the previous sections, a typical assumption in theoretical texts is that the conductivity is *homogeneous near the boundary*[7]

$$\operatorname{supp}(1-\sigma) \subset\subset D. \tag{3.2}$$

This is also a central ingredient in the proofs of the theoretical results in **[I]**, **[II]**, and **[IV]**. Under the assumption (3.2), the relative Neumann-to-Dirichlet map becomes a *smoothing operator*, so in smooth domains, it can be extended by density to $\Lambda_\sigma - \Lambda_{\mathbb{1}} : H^{-s}_\diamond(\partial D) \to H^s(\partial D)/\mathbb{R}$ for any $s \in \mathbb{R}$ [22]. This permits one to define idealized measurements with distributional current patterns, such as

$$f = \delta_p - \delta_q \ \in \ H^{-(n-1)/2-\epsilon}_\diamond(\partial D), \tag{3.3}$$

where $p, q \in \partial D$, $\epsilon > 0$, and the resulting relative potentials $u - u_{\mathbb{1}}$ are smooth on and near ∂D.

The current patterns (3.3) have a natural connection to relative EIT measurements. It was shown in [20] that *point electrode models* are the limits of CEM difference measurements as the diameter h of the electrodes tends to zero. In particular, the dual evaluation

$$\langle \delta_x - \delta_y, (\Lambda_\sigma - \Lambda_{\mathbb{1}})(\delta_p - \delta_q) \rangle \tag{3.4}$$

is the limit of a difference measurement with current-feeding electrodes at $p, q \in \partial D$ and sensing (voltage-measuring) electrodes at $x, y \in \partial D$. Furthermore, the rate of convergence is $\mathcal{O}(h^2)$. The properties of point electrode measurements of the type (3.4) as functions of $x, y, p, q \in \partial D$ (i.e., with "mobile electrodes") are the main subject of this thesis. The model (3.4) requires a smooth domain

[7] If σ is equal to any other constant than one near ∂D, the setup can be transformed to this form by scaling. Many of the presented statements also remain true if the constant is replaced by a regular enough known background $\tilde{\sigma}$.

boundary, but in [**IV**], a measure-theoretic formulation of point electrodes is introduced in order to extend the concept to piecewise smooth domains.

A particular type of measurement, dubbed *bisweep data* in [**II**], is the function $\varsigma : \partial D \times \partial D \to \mathbb{R}$,

$$\varsigma(x, y) = \langle \delta_x - \delta_y, (\Lambda_\sigma - \Lambda_{\mathbb{1}})(\delta_x - \delta_y) \rangle,$$

which is a point electrode model for all EIT measurements with only two electrodes, used for both current injection and voltage measurement. The properties of bisweep data are studied in [**II**] and [**IV**].

Articles [**I**] and [16] consider *sweep data* $\varsigma_{x_0} : \partial D \to \mathbb{R}$, $\varsigma_{x_0}(x) = \varsigma(x, x_0)$, which can be interpreted as the restriction of bisweep data where the other coordinate x_0 is held fixed. In addition to these, a modality called the *backscatter data* of EIT, $b : \partial D \to \mathbb{R}$,

$$b(x) = \langle \delta'_x, (\Lambda_\sigma - \Lambda_{\mathbb{1}})\delta'_x \rangle,$$

where $\delta'_x : \varphi \mapsto \varphi'(x)$ (derivative w.r.t. arc length parameter), $D \subset \mathbb{R}^2$, has been studied in [17][21][22][26]. The techniques utilized in the studies on sweep and backscatter data are also closely related to inverse conductivity problems with one Cauchy data pair $(f, u|_{\partial D})$ (i.e., "single measurement"; cf., e.g., [19][23][35]).

4. Inverse scattering

4.1 Helmholtz equation

The Helmholtz equation

$$\Delta u + k^2 \eta u = 0 \tag{4.1}$$

is used to describe steady states, that is, solutions of the form $U(x,t) = u(x)\tau(t)$, of the wave equation

$$\frac{\partial^2 U}{\partial t^2}(x,t) - c^2(x)\Delta_x U(x,t) = 0, \tag{4.2}$$

where $c(x)$ is the wave propagation speed of the medium at point $x \in \mathbb{R}^n$, $n = 2, 3$ (in case of a bounded time-dependent part $\tau(t) = Ae^{i\omega t} + Be^{-i\omega t}$, $A, B \in \mathbb{C}$, $\omega \in \mathbb{R}$). After normalization, one obtains (4.1), where $\eta(x) = c_0^2/c^2(x) > 0$ is the square of the *refractive index*, $c_0 > 0$ is the wave speed in the background medium, and the separation constant $k > 0$ is the *wave number*. [11]

Equation 4.1 is relevant whenever (4.2) can be used as a time-dependent model for the propagation of waves, which is often true in case of acoustic, elastic, seismic, and, in some cases, electromagnetic waves. There are also settings where (4.1) does not originate directly from (4.2). For example, one can study waves in absorbing media by letting η be complex-valued, and in quantum physics, the time-independent form of the (single-particle) *Schrödinger equation* can be written as $\Delta\Phi(x) + \frac{2m}{\hbar^2}(E - V(x))\Phi(x) = 0$ where $-V, E > 0$.

The Helmholtz equation is distinguished from other second-order elliptic equations by the positive coefficient of u (in the real-valued case). As a result, the associated bilinear forms are not coercive, which is also manifested as the existence of Dirichlet eigenfunctions, that is, non-trivial solutions to the boundary value problem $u = 0$ on ∂D for some values of k.

4.2 Forward and inverse scattering

Consider (4.1), where $\operatorname{supp}(1-\eta) \subset \mathbb{R}^n$ is bounded and $\eta \in L^\infty(\mathbb{R}^n)$ has a positive lower bound. Let $u^i \in \mathscr{C}^\infty(\mathbb{R}^n)$ be an arbitrary solution to the equation $\Delta u^i + k^2 u^i = 0$. Then there exists a unique function $u^s \in H^1_{\mathrm{loc}}(\mathbb{R}^n)$ that satisfies the *Sommerfeld radiation condition*

$$\lim_{r\to\infty} r^{(n-1)/2}\left(\frac{\partial u^s}{\partial r} - iku^s\right) = 0, \tag{4.3}$$

where $r = |x|$, and $u = u^i + u^s$ is a solution of (4.1). Here u^i is called an incident field (or incident wave), u^s the scattered field, and u the total field. This framework is known as scattering by the inhomogeneous medium η. A related configuration is scattering by an obstacle $D \subset \mathbb{R}^n$, where $\Delta u + k^2 u = 0$ in $\mathbb{R}^n \setminus \overline{D}$, and the field u satisfies some condition on the boundary of the obstacle. For instance, a *sound-soft* obstacle induces the condition $u = 0$ on ∂D. Also in obstacle scattering, one can decompose $u = u^i + u^s$, where $u^s \in H^1_{\mathrm{loc}}(\mathbb{R}^n \setminus \overline{D})$ satisfies (4.3).

The function

$$u_\infty(\hat{x}) = \lim_{r\to\infty} r^{(n-1)/2} e^{-ikr} u^s(r\hat{x}),$$

where $\hat{x} \in S^{n-1} = \{x \in \mathbb{R}^n : |x| = 1\}$, is called the *far-field* of u^s. Scattering problems are typically considered with plane waves

$$u^i(x) = u^i(x,\theta) = e^{ikx\cdot\theta},$$

$\theta \in S^{n-1}$ as the incident fields, and the function $u_\infty(\hat{x},\theta)$ comprised of the far-fields of all the corresponding scattered waves $u^s(\cdot,\theta)$ is called the *far-field pattern* (or *scattering amplitude*) of η (or, respectively, D).

One can also consider incident fields composed of plane waves from different directions, that is, *Herglotz waves*

$$u^i_f(x) = \int_{S^{n-1}} e^{ikx\cdot\theta} f(\theta)\,\mathrm{d}S_\theta.$$

The *far-field operator* $F : L^2(S^{n-1}) \to L^2(S^{n-1})$ maps f to the far-field corresponding to u^i_f, and the far-field pattern is the *Schwartz kernel* of this operator

$$\int_{S^{n-1}} g\cdot(Ff)\,\mathrm{d}S = \int_{S^{n-1}}\int_{S^{n-1}} u_\infty(\hat{x},\theta) f(\theta) g(\hat{x})\,\mathrm{d}S_\theta\,\mathrm{d}S_{\hat{x}}.$$

The properties of far-field patterns are studied in [**III**]. In particular, a fundamental property, the joint analyticity of u_∞ with respect to $\hat{x}$ and θ is proven.

In the Helmholtz equation context, an important class of *inverse scattering* problems are of the type: given (a part of) the far-field pattern u_∞, determine

the inhomogeneity η (resp. the obstacle D). Notable special cases are determining an obstacle from the far-field $u_\infty(\cdot, \theta)$ of a single incident wave or the *backscatter data* $\theta \mapsto u_\infty(-\theta, \theta)$. The data may also include measurements with different wave numbers k. Inverse scattering problems are not directly considered in this thesis. See [11] and the references therein for the basic results in this field.

5. Discussion and summary of findings

The main results of each included article are listed below.

[**I**] This article presents a method for obtaining information about the location, size, and conductivity of inclusions from sweep data of EIT. It is based on a similar method developed for EIT backscatter data by Hanke [17]. The method relies on rational Laurent–Padé approximants and is motivated by the analyticity of sweep data outside the inclusions. The article includes numerical experiments with both CEM-simulated and ideal point electrode sweep data.

[**II**] It is shown that bisweep data determines the whole Neumann-to-Dirichlet map, and thus also any measurable conductivity (satisfying eq. 3.2), in smooth plane domains. Due to the joint analyticity of bisweep data, which is also proven in this paper, this yields a new kind of partial data result for Calderón's problem in the plane.

[**III**] The techniques in [**II**] are applied to inverse scattering, which proves the joint analyticity of the far-field pattern in any dimension.

[**IV**] The concept of point electrodes is formally extended to piecewise smooth plane domains. It is shown that bisweep data are a Schwartz kernel of the relative Neumann-to-Dirichlet map (due to the factor spaces associated with the Neumann problem, there are many Schwartz kernels). The article introduces a numerical scheme for transforming the bisweep data inverse problem of a general plane domain to a standard inverse conductivity problem for the relative Neumann-to-Dirichlet map in the unit disk. Numerical examples are also presented.

The partial data results in [**II**] and [**IV**] have simpler and more elementary proofs, which are presented here for completeness.

Theorem 1. *Under the assumption* (3.2)*, the distributional measurements*

$$\langle \delta_y^{(k)}, (\Lambda_\sigma - \Lambda_{\mathbb{1}})\delta_y^{(l)} \rangle, \qquad k, l = 1, 2, 3, \ldots,$$

at any point $y \in \partial B$ determine Λ_σ, and thus the conductivity $\sigma \in L^\infty(B)$, in the unit disk B. Here $\delta_y^{(k)} : f \mapsto \frac{\partial^k}{\partial \theta^k} f(\cos\theta, \sin\theta)|_{(\cos\theta,\sin\theta)=y}$ denotes the k:th angular derivative distribution at $y \in \partial B$.

Proof. Let u^l and $u^l_{\mathbb{1}}$ be functions satisfying $\nabla \cdot (\sigma \nabla u^l) = \Delta u^l_{\mathbb{1}} = 0$ in B with the Neumann boundary condition $\partial u^l/\partial \nu = \partial u^l_{\mathbb{1}}/\partial \nu = \delta_y^{(l)}$ (cf. [22] for a rigorous definition of this statement). Then $w^l := u^l - u^l_{\mathbb{1}} \in H^1(B)/\mathbb{R}$ satisfies

$$\nabla \cdot (\sigma \nabla w^l) = \nabla \cdot ((1-\sigma)\nabla u^l_{\mathbb{1}}) \ \text{ in } B, \qquad \frac{\partial w^l}{\partial \nu} = 0 \ \text{ on } \partial B,$$

and, in particular, it is harmonic in some neighborhood of ∂B in B. Due to the homogeneous Neumann condition, w^l can be extended (by reflection) to a harmonic function in some open subset of $\mathbb{R}^2$ containing ∂B.

Therefore, $w^l|_{\partial B}$ is well-defined and analytic, so the derivatives

$$\langle \delta_y^{(k)}, (\Lambda_\sigma - \Lambda_{\mathbb{1}})\delta_y^{(l)} \rangle = \langle \delta_y^{(k)}, w^l \rangle = \frac{\partial^k}{\partial \theta^k} w^l(\cos\theta, \sin\theta)|_{(\cos\theta,\sin\theta)=y},$$

for $k = 1, 2, 3, \ldots$ determine $w^l|_{\partial B}$ up to a constant. As a result, the quantity

$$\langle g, (\Lambda_\sigma - \Lambda_{\mathbb{1}})\delta_y^{(l)} \rangle = \int_{\partial B} g w^l \, \mathrm{d}s = \langle \delta_y^{(l)}, (\Lambda_\sigma - \Lambda_{\mathbb{1}}) g \rangle$$

is determined for any $g \in L^2_\diamond(\partial B)$. Similarly, by defining w^g, it follows that $\langle f, (\Lambda_\sigma - \Lambda_{\mathbb{1}})g \rangle$ is recovered for arbitrary $f, g \in L^2_\diamond(\partial B)$, which naturally determines $\Lambda_\sigma - \Lambda_{\mathbb{1}}$ and consequently also Λ_σ. □

Theorem 2. *Let V and W be two, possibly disjoint, arbitrary, non-empty, relatively open subsets of ∂B. The measurements*

$$\langle f, \Lambda_\sigma g \rangle, \qquad f \in L^2_\diamond(V), \ g \in L^2_\diamond(W),$$

where

$$L^2_\diamond(V) := \{ f \in L^2_\diamond(\partial B) \, : \, \operatorname{supp} f \subset V \},$$

determine Λ_σ under the assumption (3.2)*.*

Proof. If $V \cap W \neq \emptyset$, define $A = V \cap W$, $h = g$ and otherwise let $A = V$, $h = 0$. In either case, the *Cauchy data* $(u|_{\partial B}, \frac{\partial u}{\partial \nu}) = (\Lambda_\sigma g, h)$, where $\nabla \cdot (\sigma \nabla u) = 0$ in B, are known on a non-empty, relatively open subset A of ∂B.

It is well-known that the Cauchy data determine u on some relatively open neighborhood U of ∂B in B such that u is harmonic in U. Thus one recovers the whole boundary function $u|_{\partial B} = \Lambda_\sigma g$. As in the proof of Theorem 1, the self-adjointness of Λ_σ can be used to deduce that $\langle g, \Lambda_\sigma p\rangle$ is determined for any $p \in L^2_\diamond(\partial B)$, and it follows by the same arguments as before that $\Lambda_\sigma p$ is recovered up to a constant on the whole boundary ∂B. □

The above theorems are formulated in the unit disk $D = B$ for simplicity. However, the proof of Theorem 2 is valid in any domain (and dimension) as long as the unique continuation of Cauchy data can be applied. Theorem 1 can be extended to other smooth plane domains by the methods used in [**II**].

Bibliography

[1] Astala, K., and Päivärinta, L. Calderón's inverse conductivity problem in the plane. *Ann. of Math. 163*, 1 (2006), 265–300.

[2] Borcea, L. Electrical impedance tomography. *Inverse Probl. 18* (2002), R99.

[3] Browder, F. Real analytic functions on product spaces and separate analyticity. *Canad. J. Math. 13* (1961), 650–656.

[4] Brühl, M. Explicit characterization of inclusions in electrical impedance tomography. *SIAM J. Math. Anal. 32* (2001), 1327.

[5] Brühl, M., and Hanke, M. Numerical implementation of two noniterative methods for locating inclusions by impedance tomography. *Inverse Probl. 16*, 4 (2000), 1029–1042.

[6] Calderón, A. On an inverse conductivity problem. In *Seminar on Numerical Analysis and its Applications to Continuum Physics (Río de Janeiro, 1980)*, Soc. Brasil. Mat., pp. 65–73.

[7] Cheney, M., Isaacson, D., and Newell, J. Electrical impedance tomography. *SIAM Rev.* (1999), 85–101.

[8] Cheney, M., Isaacson, D., Newell, J., Simske, S., and Goble, J. NOSER: An algorithm for solving the inverse conductivity problem. *Int. J. Imag. Syst. Tech. 2*, 2 (1990), 66–75.

[9] Cheng, K.-S., Isaacson, D., Newell, J., and Gisser, D. G. Electrode models for electric current computed tomography. *IEEE Trans. Biomed. Eng. 36*, 9 (1989), 918–924.

[10] Colton, D., Coyle, J., and Monk, P. Recent developments in inverse acoustic scattering theory. *SIAM Rev. 42*, 3 (2000), 369–414.

[11] Colton, D., and Kress, R. *Inverse acoustic and electromagnetic scattering theory.* Springer, 1998.

[12] Costabel, M., and Dauge, M. A singularly perturbed mixed boundary value problem. *Commun. Part. Diff. Eq. 21*, 11 (1996), 1919–1950.

[13] Dardé, J., Hakula, H., Hyvönen, N., and Staboulis, S. Fine-tuning electrode information in electrical impedance tomography. *Inverse Probl. Imag. 6*, 3 (2012), 399–421.

[14] Dardé, J., Hyvönen, N., Seppänen, A., and Staboulis, S. Simultaneous reconstruction of outer boundary shape and admittivity distribution in electrical impedance tomography. *SIAM J. Imaging Sci. 1*, 6 (2013), 176–198.

[15] Gebauer, B., and Hyvönen, N. Factorization method and irregular inclusions in electrical impedance tomography. *Inverse Probl. 23*, 5 (2007), 2159–2170.

[16] Hakula, H., Harhanen, L., and Hyvönen, N. Sweep data of electrical impedance tomography. *Inverse Probl. 27*, 11 (2011), 115006.

[17] Hanke, M. Locating several small inclusions in impedance tomography from backscatter data. *SIAM Journal on Numerical Analysis 49* (2011), 1991–2016.

[18] Hanke, M., and Brühl, M. Recent progress in electrical impedance tomography. *Inverse Probl. 19*, 6 (2003), S65–S90.

[19] Hanke, M., Harhanen, L., Hyvönen, N., and Schweickert, E. Convex source support in three dimensions. *BIT 52*, 1 (2012), 45–63.

[20] Hanke, M., Harrach, B., and Hyvönen, N. Justification of point electrode models in electrical impedance tomography. *Math. Models Methods Appl. Sci. 21* (2011), 1395–1413.

[21] Hanke, M., Hyvönen, N., and Reusswig, S. An inverse backscatter problem for electric impedance tomography. *SIAM J. Math. Anal. 41* (2009), 1948–1966.

[22] Hanke, M., Hyvönen, N., and Reusswig, S. Convex backscattering support in electric impedance tomography. *Numer. Math.* (2011), 1–24.

[23] Harhanen, L., and Hyvönen, N. Convex source support in half-plane. *Inverse Probl. Imaging 4*, 3 (2010), 429–448.

[24] Harrach, B., and Seo, J. Detecting inclusions in electrical impedance tomography without reference measurements. *SIAM J. Appl. Math 69*, 6 (2009), 1662–1681.

[25] Heikkinen, L. M., Vilhunen, T., West, R. M., and Vauhkonen, M. Simultaneous reconstruction of electrode contact impedances and internal electrical properties: II. Laboratory experiments. *Meas. Sci. Technol. 13*, 12 (2002), 1855–1861.

[26] Hollborn, S. Reconstructions from backscatter data in electric impedance tomography. *Inverse Probl. 27* (2011), 045007.

[27] Hörmander, L. *An introduction to complex analysis in several variables*. North-Holland, Amsterdam, 1973.

[28] Hyvönen, N. Approximating idealized boundary data of electric impedance tomography by electrode measurements. *Math. models methods appl. sci. 19*, 07 (2009), 1185–1202.

[29] Imanuvilov, O. Y., Uhlmann, G., and Yamamoto, M. Inverse boundary value problem by partial data for the Neumann-to-Dirichlet-map in two dimensions. arXiv preprint arXiv:1210.1255.

[30] Imanuvilov, O. Y., Uhlmann, G., and Yamamoto, M. The Calderón problem with partial data in two dimensions. *J. Amer. Math. Soc. 23* (2010), 655–691.

[31] Isaacson, D., and Isaacson, E. Comment on Calderón's paper: "On an inverse boundary value problem". *Math. Comp 52* (1989), 553–559.

[32] Isaacson, D., Mueller, J. L., Newell, J. C., and Siltanen, S. Reconstructions of chest phantoms by the D-bar method for electrical impedance tomography. *IEEE Trans. Med. Imag. 23*, 7 (2004), 821–828.

[33] Isakov, V. *Inverse Problems for Partial Differential Equations*, 2nd ed. Springer Verlag, 1998.

[34] Jarnicki, M., and Pflug, P. *Separately analytic functions*. European Mathematical Society, 2011.

[35] Kang, H., and Lee, H. Identification of simple poles via boundary measurements and an application of EIT. *Inverse Probl. 20* (2004), 1853–1863.

[36] Kenig, C. E., and Salo, M. Recent progress in the Calderon problem with partial data. arXiv preprint arXiv:1302.4218.

[37] Kenig, C. E., Sjöstrand, J., and Uhlmann, G. The Calderón problem with partial data. *Ann. of Math.* (2007), 567–591.

[38] Kirsch, A. Characterization of the shape of a scattering obstacle using the spectral data of the far field operator. *Inverse Probl. 14*, 6 (1998), 1489–1512.

[39] Knudsen, K., Lassas, M., Mueller, J., and Siltanen, S. Regularized D-bar method for the inverse conductivity problem. *Inverse Probl. Imag. 3* (2009), 599–624.

[40] Kohn, R., and Vogelius, M. Determining conductivity by boundary measurements. *Comm. Pure Appl. Math. 37*, 3 (1984), 289–298.

[41] Kohn, R. V., and Vogelius, M. Determining conductivity by boundary measurements II. Interior results. *Comm. Pure Appl. Math. 38*, 5 (1985), 643–667.

[42] Kolehmainen, V., Vauhkonen, M., Karjalainen, P. A., and Kaipio, J. P. Assessment of errors in static electrical impedance tomography with adjacent and trigonometric current patterns. *Physiological Measurement 18*, 4 (1997), 289–303.

[43] Krantz, S., and Parks, H. *A Primer of Real Analytic Functions*. Birkhäuser, 2002.

[44] Krantz, S. G. *Function theory of several complex variables*, 2nd ed. Wadsworth & Brooks/Cole Advanced Books & Software, 1992.

[45] Lechleiter, A. A regularization technique for the factorization method. *Inverse Probl. 22*, 5 (2006), 1605–1625.

[46] Lechleiter, A., and Rieder, A. Newton regularizations for impedance tomography: a numerical study. *Inverse Probl. 22*, 6 (2006), 1967–1987.

[47] Nachman, A. Global uniqueness for a two-dimensional inverse boundary value problem. *Ann. of Math. 143* (1996), 71–96.

[48] Necas, J. *Direct methods in the theory of elliptic equations*. Springer, 2012.

[49] Seiskari, O. Locating multiple inclusions from sweep data of electrical impedance tomography. Master's thesis, Aalto University, Department of Mathematics and Systems Analysis, 2011.

[50] Somersalo, E., Cheney, M., and Isaacson, D. Existence and uniqueness for electrode models for electric current computed tomography. *SIAM J. Appl. Math 52*, 4 (1992), 1023–1040.

[51] Sylvester, J., and Uhlmann, G. A global uniqueness theorem for an inverse boundary value problem. *Ann. of Math. 125*, 2 (1987), 153–169.

[52] Uhlmann, G. Electrical impedance tomography and Calderón's problem. *Inverse Probl. 25* (2009), 123011.

[53] Vilhunen, T., Kaipio, J. P., Vauhkonen, P. J., Savolainen, T., and Vauhkonen, M. Simultaneous reconstruction of electrode contact impedances and internal electrical properties: I. Theory. *Meas. Sci. Technol. 13*, 12 (2002), 1848–1854.

Aalto-DD 165/2013

ISBN 978-952-60-5383-7
ISBN 978-952-60-5384-4 (pdf)
ISSN-L 1799-4934
ISSN 1799-4934
ISSN 1799-4942 (pdf)

Aalto University
School of Science
Department of Mathematics and Systems Analysis
www.aalto.fi

BUSINESS +
ECONOMY

ART +
DESIGN +
ARCHITECTURE

SCIENCE +
TECHNOLOGY

CROSSOVER

**DOCTORAL
DISSERTATIONS**